Motility Induced Phase Separation and Frustration in Active Matter Swarmalators

B. Adorjáni[1], A. Libál[1], C. Reichhardt[2], and C. J. O. Reichhardt[2]

[1] *Mathematics and Computer Science Department, Babeş-Bolyai University, Cluj 400084, Romania*
[2] *Theoretical Division and Center for Nonlinear Studies,*
Los Alamos National Laboratory, Los Alamos, New Mexico 87545, USA
(Dated: September 21, 2023)

We introduce a system of active matter swarmalators composed of elastically interacting run-and-tumble active disks with an internal phase ϕ_i. The disks experience an additional attractive or repulsive force with neighboring disks depending upon their relative difference in ϕ_i. In the absence of the internal phase, the system forms a Motility-Induced Phase Separated (MIPS) state, but when the swarmalator interactions are present, a wide variety of other active phases appear depending upon whether the interaction is attractive or repulsive and whether the particles act to synchronize or anti-synchronize their internal phase values. These include a gas-free gel regime, arrested clusters, a labyrinthine state, a regular MIPS state, a frustrated MIPS state for attractive anti-synchronization, and a superlattice MIPS state for attractive synchronization.

I. INTRODUCTION

Active matter systems contain self-motile particles and can be found in soft matter [1–3], biological [4–8], social [9, 10], active topological [11, 12], and robotic [13–15] contexts. The simplest models of active matter consist of interacting elastic disks undergoing a run-and-tumble motion or driven Brownian diffusion. Even in the absence of any attractive forces, such motion produces what is known as Motility Induced Phase Separation (MIPS) when the activity level and the disk density are sufficiently large [16–24]. For monodisperse particles, the dense clusters in the MIPS state have triangular order and coexist with a lower density gas. An open question is whether there can be other types of MIPS regimes that have alternative ordering within the clusters. Also unknown is whether inclusion of more complex particle-particle interactions can lead to a comprehensive way to connect different MIPS regimes within one model.

In many soft and condensed matter systems that have competing or multi-length scale interactions, additional larger scale patterning can arise [25–30]. Frustration effects can occur when not all of the constraints in the system can be satisfied simultaneously, as is the case for proton ordering in water ice [31], frustrated colloidal systems [32, 33], spin ice [34], artificial spin ice systems [35, 36], and certain types of metamaterials [37]. There are potentially many active systems where additional competing interactions could be added that would create additional regimes or frustration effects that might interfere with the crystalline ordering in the dense phase of MIPS.

Here we consider a model of run-and-tumble active disks that exhibit a MIPS phase for sufficiently high activity and density. We give each disk an internal phase ϕ_i and introduce an additional attractive or repulsive force between neighboring disks i and j based on the swarmalator rules for internal phase differences $\delta\phi_{ij}$ [38]. This internal phase evolves as a function of time and also changes due to interactions with neighboring disks located within a radius $2r_{\rm sw}$. A schematic illustration of the model appears in Fig. 1. The parameter J controls the strength and sign of the translational force exerted along the line connecting two disks i and j depending on the magnitude of $\delta\phi_{ij}$. A second parameter K determines how rapidly the value of ϕ_i changes in response to $\delta\phi_{ij}$, with positive values of K resulting in a net reduction of $\delta\phi_{ij}$ and negative K values causing $\delta\phi_{ij}$ to increase. With these additional interactions, we find that a wide variety of active matter regimes can be realized, including distinctive MIPS states that revert back to the ordinary MIPS state in the limit $J = 0$, $K = 0$. For $J > 0$, the MIPS state contains a hexagonal superlattice structure of disks with similar phase values surrounded by a gas of misaligned disks. We also observe a multi-phase gel state at $K = 0$ and a frustrated liquid at high K values where the superlattice is unable to form. We map the evolution of these distinct states as a function of activity and density and find that MIPS is enhanced for the combination $K < 0$ and $J > 0$, but is suppressed for other combinations.

Our model could be realized using robotic swarms with steric interactions and swarmalator rules [39, 40]. Similar interactions could arise for biological systems of motile cells of different types in which individual cells are attracted to one cell type but repelled by a different cell type [41]. There are also a variety of soft matter systems that can have particle-specific or competing attractive and repulsive interactions with each other or that have multiple length scales in their interactions, which can create pattern forming states [25–27, 30, 42, 43]. It should also be feasible to create competing interactions using light activated colloids with feedback loops [44–46].

II. MODEL

We consider a two-dimensional system of size $S_x = 160$ and $S_y = 160$ with periodic boundary conditions in the x and y directions containing $N = 4000$ circular disks of radius of $R_d = 1.0$. The disk density is given by $\rho = N\pi R_d^2/(S_x S_y)$. As shown in Fig. 1(a), disk i interacts sterically at short range with other disks according to
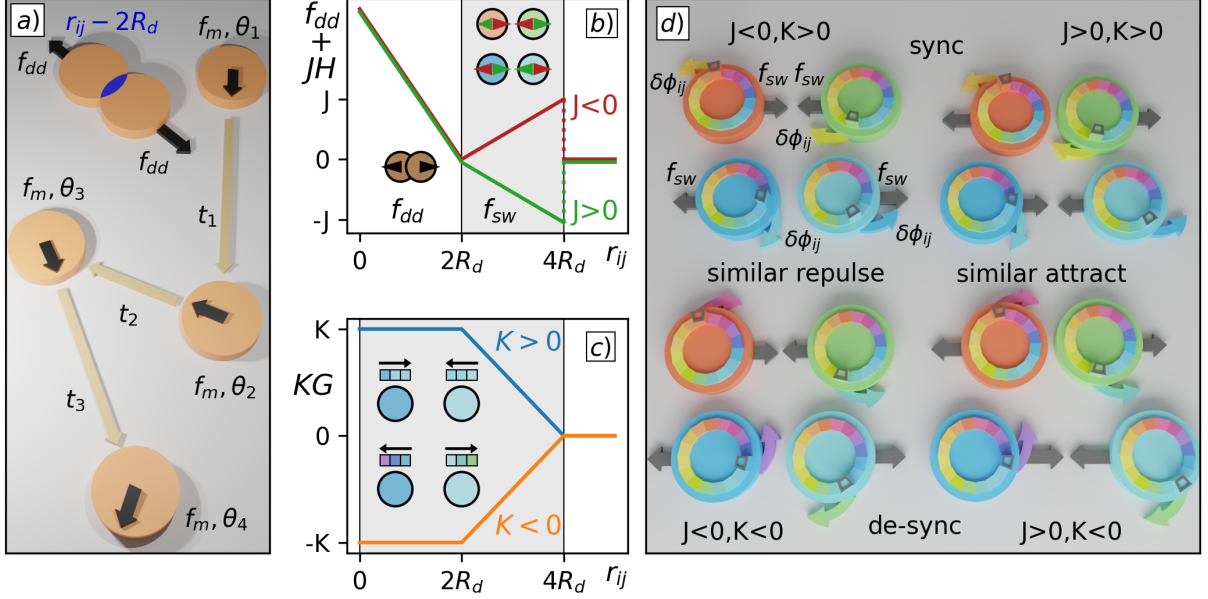
FIG. 1. Schematics of the system and the disk-disk interactions. (a) Colliding disks experience a steric repulsion force $f_{\rm dd}$. Each disk also undergoes run-and-tumble motion with a motor force of $f_{\rm m}$ directed along θ_i for a time t_i, and new values of θ_i and t_i are selected during each instantaneous tumbling event. (b) $f_{\rm dd} + JH$, the disk-disk forces and the function $JH(r_{ij})$, vs the distance r_{ij} between disks. Only steric disk repulsion acts when $r_{ij} \leq 2R_d$. The value of $JH(r_{ij})$ becomes nonzero when $2R_d < r_{ij} \leq 4R_d$; it is negative when $J > 0$ (green) and positive when $J < 0$ (red). The left inset shows the steric interactions (brown disks). The upper center inset shows swarmalator interactions between disks of different phase, which is repulsive for $J > 0$ (green arrows) and attractive for $J < 0$ (red arrows). The lower center inset shows the swarmalator interactions when the disks have similar phases, which is attractive for $J > 0$ (green arrows) and repulsive for $J < 0$ (red arrows). (c) The function $KG(r_{ij})$ controlling the phase evolution. When $K > 0$ (blue), the phase of neighboring disks becomes synchronized over time, as illustrated by the boxes in the top inset that illustrate how the phase changes as a function of time. When $K < 0$ (orange), disk phases become desynchronized over time, as shown by the boxes in the lower inset. (d) Summary of swarmalator forces for the four possible nonzero combinations of J and K. Disk color indicates the value of the phase, and the possible phase values appear as a ring inside each disk. Grey arrows show the orientation of $f_{\rm sw}$ for each combination, while the curved colored arrows indicate the direction in which the phase will evolve as a result of the interaction. For each combination, the phases of the disk pairs are different in the upper row and similar in the lower row.

$\mathbf{f}_{\rm dd} = f_{\rm dd}\hat{\mathbf{r}}_{ij}$ with $f_{\rm dd} = \sum_j^N k(2R_d - r_{ij})\Theta(2R_d - r_{ij})$, where $r_{ij} = |\mathbf{r}_j - \mathbf{r}_i|$ is the distance between the centers of disks i and j, $\hat{\mathbf{r}}_{ij} = (\mathbf{r}_j - \mathbf{r}_i)/r_{ij}$, Θ is the Heaviside step function, and $k = 20.0$ is the elastic constant. Run-and-tumble motion is produced by a motor force $\mathbf{f}_m$ of magnitude $f_m = 1$ that is directed along $\theta_i \in [0, 2\pi)$ during a time $t_i \in [\tau, 2\tau]$. At the end of each running event, an instantaneous tumbling event occurs in which new values of θ_i and t_i are chosen randomly from the allowed intervals.

Each particle is endowed with an internal phase $\phi_i \in [0, 2\pi)$ that is not coupled to θ_i. The internal phase undergoes a slow thermal diffusion that is independent of the surroundings of the disk. The thermal force F_i^T is implemented using Langevin kicks with the properties $\langle F_i^T \rangle = 0$ and $\langle F_i^T(t)F_i^T(t') \rangle = 2k_B T\delta_{ij}\delta(t-t')$. Here we use a small thermal force magnitude of $F^T = 0.001$. The value of ϕ_i is also modified by a forcing term of strength K that is dependent on the relative phases $\delta_{ij} = (\phi_j - \phi_i)$ of neighboring disks within a radius of $r_{ij} \leq 2r_{\rm sw}$ where

$r_{\rm sw} = 2R_d$. This gives:

$$\frac{d\phi_i}{dt} = \sum_j^N K \sin(\delta\phi_{ij})G(r_{ij}) + F_i^T \quad (1)$$

where $G(r_{ij}) = 1$ for $r_{ij} \leq r_{\rm sw}$, $G(r_{ij}) = (2r_{\rm sw} - r_{ij})/r_{\rm sw}$ for $r_{\rm sw} < r_{ij} \leq 2r_{\rm sw}$, and $G(r_{ij}) = 0$ for $r_{ij} > 2r_{\rm sw}$. The form of $G(r_{ij})$ is illustrated in Fig. 1(c). When $K > 0$, the phases of neighboring disks tend to become synchronized, while when $K < 0$, the phases tend to become anti-synchronized.

The positions of the disk centers are obtained by integrating the following equation of motion:

$$\eta\frac{d\mathbf{r}_i}{dt} = \mathbf{f}_m + \mathbf{f}_{\rm dd} + \mathbf{f}_{\rm sw} \quad (2)$$

where we set the damping coefficient to $\eta = 1$. The swarmalator interaction force is given by $\mathbf{f}_{\rm sw} = f_{\rm sw}\hat{\mathbf{r}}_{ij}$ with

$$f_{\rm sw} = -\sum_j^N J\cos(\delta\phi_{ij})H(r_{ij}) \ , \quad (3)$$
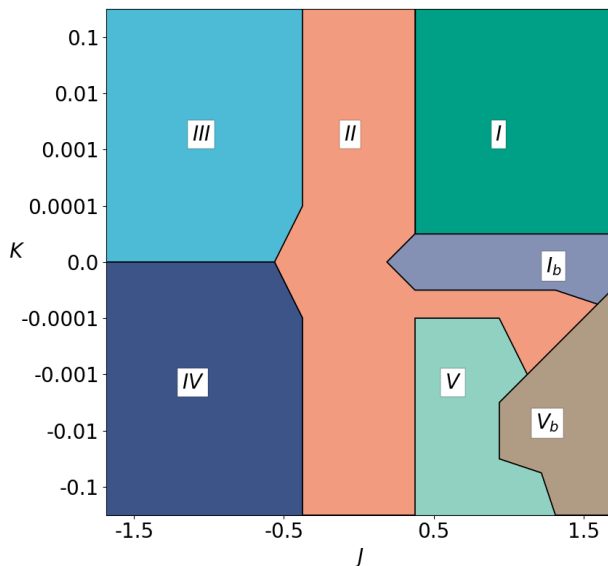
FIG. 2. Dynamic phase diagram as a function of K, the synchronization factor, and J, the swarmalator force strength, for an active disk system with a density of $\rho = 0.49$ at $\tau = 1.5 \times 10^5$. Region I with $K > 0$ and $J > 0$ is the active gel where all of the disks synchronize to the same phase, as shown in Fig. 3(a). Region II is the ordinary MIPS phase for $J = 0$, illustrated in Fig. 3(h). Region III for $J < 0$ and $K > 0$ is the active labyrinthine state shown in Fig. 3(b) where the disks synchronize to the same phase. In region IV for $K < 0$ and $J < 0$ we find the frustrated MIPS phase illustrated in Fig. 3(c,e) with stripe ordering in the clusters, while region V for $K < 0$ and $J > 0$ is a superlattice MIPS phase as shown in Fig. 3(d,f). Region I_b is the arrested gel phase shown in Fig. 4(a), and region V_b is a frustrated cluster fluid, illustrated in Fig. 4(b).

where $H(r_{ij}) = 0$ for $r_{ij} \leq r_{\mathrm{sw}}$ or $r_{ij} > 2r_{\mathrm{sw}}$ and $H(r_{ij}) = (r_{ij} - r_{\mathrm{sw}})/r_{\mathrm{sw}}$ for $r_{\mathrm{sw}} < r_{ij} \leq 2r_{\mathrm{sw}}$. As shown in Fig. 1(b), disks with similar phase repel each other when $J < 0$ and attract each other when $J > 0$. When $J = 0$, the internal phase has no impact on the disk dynamics and the model reverts to the normal MIPS behavior found in the absence of swarmalator interactions. Figure 1(d) summarizes the four possible interaction regimes for nonzero combinations of J and K.

We numerically integrate equations (1) and (2) using a simulation time step of $dt = 0.001$. To initialize the sample, we place all disks in randomly chosen non-overlapping positions and set the initial values of θ_i, ϕ_i, and t_i to random values chosen from the allowed range of each quantity. We allow the system to evolve for 2×10^6 simulation time steps before collecting data during the next 3×10^6 simulation time steps.

III. RESULTS

In Fig. 2, we plot a dynamic phase diagram for samples with $\rho = 0.49$ and $\tau = 1.5 \times 10^5$ as a function of K versus J, where we highlight the seven regimes of behavior. For this choice of τ, an isolated disk undergoing no collisions would travel a distance d_{free} ranging from $d_{\mathrm{free}} = 150$ to $d_{\mathrm{free}} = 300$, comparable to the system size. When $K = 0$ and $J = 0$ the system forms an ordinary MIPS state, which we designate as region II. This MIPS phase extends along the $J = 0$ axis for all values of K, since the swarmalator interaction has no effect on the disk motion when $J = 0$. The MIPS state persists for small values of $|J|$ when the swarmalator force remains too small to perturb the motion significantly. In region I, where $J > 0$ and $K > 0$, all of the disks evolve to have the same internal phase ϕ_{bulk}, the swarmalator force becomes attractive, and a gas-free gel state emerges, as illustrated in Fig. 3(a). We find the same gel state for most choices of τ and ρ, but as τ increases, the gel forms more rapidly. The value of ϕ_{bulk} differs depending on the initial conditions, but all of the disks always reach $\phi_i = \phi_{\mathrm{bulk}}$ after a transient time that becomes longer as K becomes smaller. At $K = 0$, for small but positive J we find region I_b where there is no global ordering of ϕ_i. Instead, small, gel-like clusters of coherent phase form with no surrounding free gas state, as shown in Fig. 4(a,c). In both regions I and I_b, the gel clusters slowly drift through the system as a result of the disk activity.

For $K > 0$ and $J < 0$ in Fig. 2, we find region III where the disks synchronize to a single global internal phase value ϕ_{bulk} but repel each other. Here a labyrinthine pattern appears, as illustrated in Fig. 3(b). Due to the activity, region III has some characteristics of a fluctuating fluid. The disks do not form a crystal because the repulsive swarmalator force drops to zero when the particles touch ($r_{ij} = 2R_d$) and is maximal when $r_{ij} = 4R_d$. The labyrinthine structures are similar to the labyrinthine and cluster phases found in systems with multiple length scale repulsive potentials [26, 42]. In our case, there is a core repulsive force from the elastic repulsion extending out to $r_{ij} = 2R_d$ that is surrounded by a softer intermediate range swarmalator repulsive force from $2R_d < r_{ij} \leq 4R_d$. In non-active systems where this type of two-step repulsion is present, a range of additional crystalline and stripe-like phases appear for varied densities [26, 27]; however, the activity in our system prevents the formation of such higher-order structures.

For $K < 0$ and $J < 0$ we observe a frustrated MIPS state that we denote region IV in Fig. 2. This consists of a high-density solid with stripe-like internal phase ordering coexisting with a fluid that contains locally phase ordered patches, as shown in Fig. 3(c). A blow up in Fig. 3(f) of one of the dense regions indicates that disks with a given value of ϕ_i form stripes that are interleaved between disks with the opposite phase. A considerable number of lattice defects are present in the dense patches and the internal phases are continuously changing due to the ac-
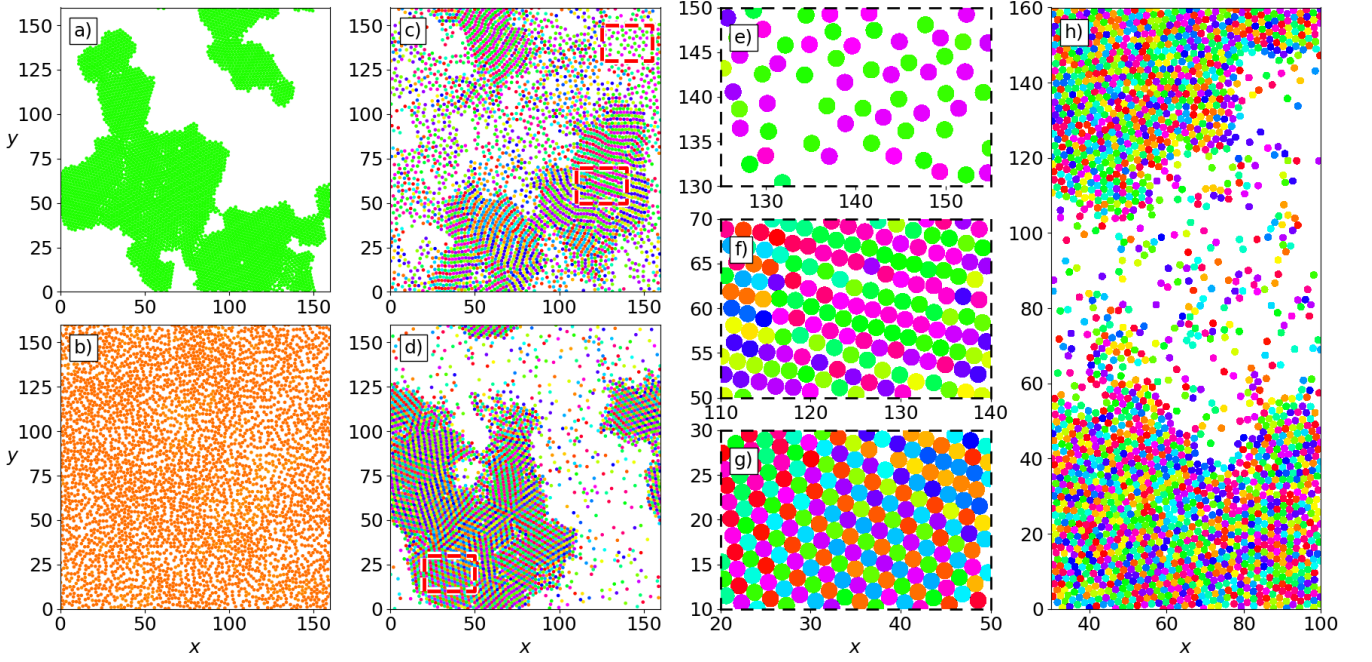
FIG. 3. Illustrations of the disk locations (circles) and internal phases (indicated by color) for the dynamic phases described in Fig. 2 in a system with $\rho = 0.49$ and $\tau = 1.5 \times 10^5$. (a) Region I, the gel state where all disks have the same value of ϕ_i, at $J = 1.0$ and $K = 0.1$. (b) Region III, the fluid labyrinthine state where all disks have the same value of ϕ_i, at $J = -1$ and $K = 0.001$. (c) Region IV, the frustrated MIPS state with stripe ordering of ϕ_i inside the clusters, at $J = -1.5$ and $K = -0.1$. (d) Region V, the superlattice MIPS state, at $J = 1.0$ and $K = -0.1$. (e) A blowup of the upper red dashed box in panel (c) showing the phase correlated fluid portion of the frustrated MIPS state. (f) A blowup of the lower red dashed box in panel (c) showing stripe ordering in the dense portion of the frustrated MIPS state. (g) A blowup of the red dashed box in panel (d) showing a detail of the superlattice ordering in the superlattice MIPS state. (h) Region II, the MIPS state with no phase ordering, at $J = 0$ and $K = 0$. Videos of these phases are available in the supplemental material.

tivity. Within region IV, the disks are attempting to anti-synchronize their internal phase with the phases of the neighboring particles. Once this anti-synchronization is successful, the disk is attracted to its neighbors, but disks with the same value of ϕ_i repel each other. Formation of the striped phase ordering is favored because this allows each disk to maximize the number of nearest neighbors with attractive interactions while minimizing the number of neighbors with repulsive interactions. The internal phase ordering pattern resembles the patterns found for frustrated spins on a hexagonal lattice or the buckling of colloidal particles that have been packed into slightly more than a monolayer [32, 47, 48]. In the case of the colloidal system, the colloidal particles are a little too dense to form a triangular solid, but can maintain their triangular arrangement by buckling out of plane, giving each particle an effective spin degree of freedom and permitting the system to form an antiferromagnetic Ising-like state that is frustrated on a hexagonal lattice. The frustrated state breaks up into multiple stripe-like domains that each have different orientations of the buckled pattern.

Although region IV is related to a MIPS state, it has a larger number of disks in the gas state compared to ordinary MIPS and these disks exhibit a local phase ordering, as illustrated in Fig. 3(e). The gas phase particles form loose pairs that have opposite values of ϕ_i. This ordering occurs only very locally and the specific values of ϕ_i for the opposing pairs vary from one gaseous patch to the next. Although this locally ordered liquid structure is preferred by the system at low densities, it is susceptible to the shear and compression produced by the activity of the disks, so it does not remain stable as a function of time but forms and disintegrates constantly in order to establish a dynamical equilibrium with the dense striped crystalline patches.

For $J > 0$ and $K < 0$, the system forms a more stable superlattice MIPS state, termed region V, where the dense regions develop a hexagonal superlattice ordering, illustrated in Fig. 3(d). For these parameters, disks with the same phase attract each other and disks with the opposite phase repel each other, but the phases of neighboring disks evolve to be different from each other. To minimize the competition between attractive and repulsive interactions, the system forms the dense hexagonal superlattice ordering shown in more detail in Fig. 3(g). The swarmalator force decreases as r_{ij} decreases and vanishes when $r_{ij} = 2R_d$, so disks that are in direct contact can avoid being repelled by each other. Locally the system then resembles repulsively interacting internal phases on
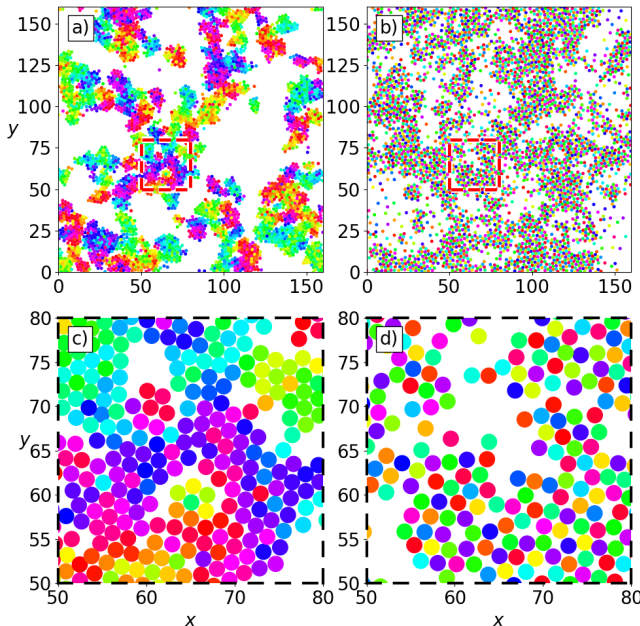
FIG. 4. Illustrations of the disk locations (circles) and internal phases (indicated by color) for the phases I_b and V_b in Fig. 2 for a system with $\rho = 0.49$ and $\tau = 1.5 \times 10^5$. (a) Region I_b or the arrested gel state at $J = 1.5$ and $K = 0$, where the system separates into clusters with the same internal phase but cannot fully coarsen due to the repulsive interactions between disks with opposite phases. (b) Region V_b, the fluctuating clump state with local anti-synchronized phase ordering, at $J = 1.5$ and $K = -0.01$. (c) A blowup of the red dashed box for region I_b in panel (a). (d) A blowup of the red dashed box for region V_b in panel (b).

a triangular lattice, and the superlattice ordering emerges from the synchronization of the evolution of neighboring phases.

In Fig. 3(h), we show the regular MIPS state or region II at $K = 0$ and $J = 0$, where the disks maintain the same random phases they received during initialization; however, since the internal phases play no role in the dynamics, the dense region develops no phase ordering. The regular MIPS state extends along the K axis for a band of finite width in J, since when J is sufficiently weak the evolution of the internal phases does not change the disk dynamics. We also find a window of region II for larger positive J and small but finite negative K; here, the anti-synchronization is not strong enough to alter the internal phases and produce region V or V_b behavior.

In Fig. 4(a), we illustrate the configuration for what we call region I_b or the phase arrested gel, which occurs for $K = 0$ and $J > 1$. In this case, the system starts with the disks assigned to random phases, but since $K = 0$ these phases cannot evolve with time, so the system can be viewed as containing active particles that have randomized attractive and repulsive interactions with each other. Over time, the disks segregate into clumps of uniform phase, but formation of a single clump as in the

gel state or region I is not possible because clumps with opposite phase repel each other. A blow up of this state appears in Fig. 4(c). The frustrated clump fluid or region V_b that appears for $K < 0$ and $J > 1.5$ is illustrated in Fig. 4(b). The internal phase configuration is not ordered within the solid clumps and the clusters are less compact and show larger fluctuations than the region II regular MIPS state. Although there is no superlattice ordering within the cluster, particles with the same phase generally try not to be next to each other. This region appears when J becomes large enough that the repulsive and attractive forces destabilize the solid that forms in region V.

The different regimes can be distinguished using several measures. The circularly averaged internal phase is given by

$$\bar{\phi} = \frac{1}{N} \sum_{i=1}^{N} \phi_i \ . \tag{4}$$

This quantity is calculated every 5000 simulation time steps and we then compute the time average $\langle \bar{\phi} \rangle$ from $M = 600$ measurements. We obtain the standard deviation $\sigma = \sqrt{\sum_k^M (\bar{\phi}_k - \langle \bar{\phi} \rangle)^2 / (M-1)}$, and plot a heat map of σ as a function of K versus J in Fig. 5(a). For $K > 0$, σ drops to zero since all of the internal phases synchronize to a global value ϕ_{bulk}. For $K = 0$, σ takes on a small finite value since the small thermal fluctuations of the individual internal phases are no longer suppressed by synchronization, while for $K < 0$, σ becomes large since the disks evolve to have phases opposite from those of their neighbors.

We define the average frustration f as the sum,

$$f = \left\langle \frac{1}{N} \sum_{i=1}^{N} f_i \right\rangle \ , \tag{5}$$

of the individual disk frustration values f_i,

$$f_i = -\frac{1}{n} \operatorname{sgn}(J) \operatorname{sgn}(K) \sum_{j=1}^{N} \cos(\delta\phi_{ij}) \Theta(4R_d - r_{ij}) \ , \tag{6}$$

where the average is taken over time. An individual disk with no frustration has $f_i = -1$. Examples where frustration does not occur include disks in region II with $J = 0$ and $K = 0$, disks that have no neighbors within a radius $r_{ij} = 4R_d$, or disks for which all of the neighbors satisfy both the J and K interactions such as in the gel state of region I. In Fig. 5(b) we plot a heat map of f, which ranges from $-1 \leq f \leq 1$, as a function of K versus J. We find $f = +1$ (maximum frustration) in region III where the internal phases are aligned but the swarmalator interaction forces are repulsive. In the frustrated MIPS state of region IV, f is close to zero but negative, indicating intermediate frustration, while in region V or the superlattice MIPS state, the frustration is intermediate but positive. Generally, as f gets closer to $f = +1$, the motion in the system becomes more fluid-like.
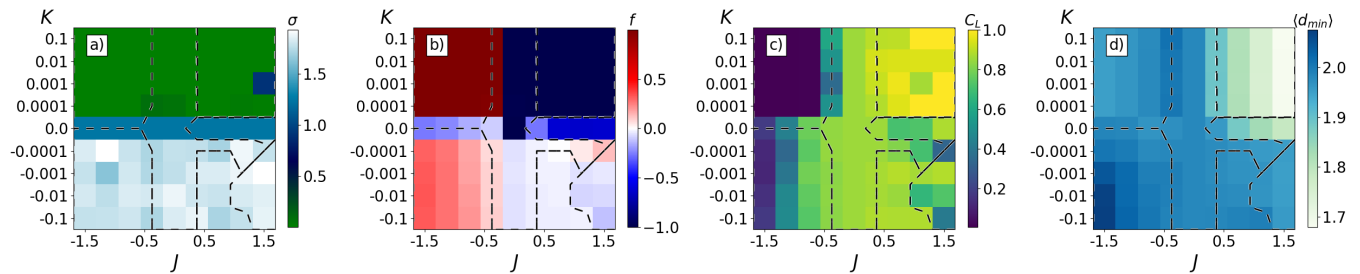
FIG. 5. Illustration of different measurements that can be used to quantify the appearances of the different regimes. Each is plotted as a heat map as a function of K vs J in a system with $\rho = 0.49$ and $\tau = 1.5 \times 10^5$. (a) Standard deviation σ of the circularly averaged phase $\bar{\phi}$ of the disks. (b) The average frustration f. (c) Fraction C_L of disks contained in the largest cluster present in the system. (d) The average shortest distance $\langle d_{\min} \rangle$ between neighboring disks.

The average fraction C_L of disks in the largest cluster is defined by identifying groups of disks that are all in steric contact with each other as members of a single cluster. This quantity is computed using an efficient neighbor lookup table method [49] and is then averaged over time. In Fig. 5(c) we plot a heat map of C_L as a function of K versus J. In the active gel region I, C_L is large, while in the active labyrinthine region III, C_L is low since the repulsive swarmalator forces break the labyrinth structures into small disjoint clusters. For the MIPS-like regions IV and V, there is a substantial amount of clustering but C_L is lower than its value in the standard MIPS region III. We observe reduced clustering in region V_b, and the value of C_L is one of the criteria that we use to distinguish region V_b from region V.

In systems where pattern formation is possible, the average distance to the closest neighbor $\langle d_{\min} \rangle$ can be used to identify signatures of different patterns [43]. The closest neighbor of disk i is at a distance $d^i_{\min} = \min\{r_{ij}\}$ and we obtain $\langle d_{\min} \rangle = \langle N^{-1} \sum_i^N d^i_{\min} \rangle$, where the average is taken over time. Figure 5(d) shows a heat map of $\langle d_{\min} \rangle$ plotted as a function of K versus J. In the active gel region I, $\langle d_{\min} \rangle$ is small since all of the disks are in one giant cluster and the swarmalator force acts as a surface tension that further compresses the disks. There is a linear dependence of $\langle d_{\min} \rangle$ on J in the active labyrinthine region III since the increasing repulsion slightly reduces the size of the small clusters that appear in the labyrinth formation. In the frustrated MIPS region IV, $\langle d_{\min} \rangle$ reaches its lowest value for large J and K where the stripe-ordered dense clusters illustrated in Fig. 3(f) coexist with the maximum amount of the low density phase-correlated state shown in Fig. 3(e). We used the values of σ, f, C_L, and $\langle d_{\min} \rangle$ to construct the dynamic phase diagram plotted in Fig. 2.

We next consider the impact of changing the activity τ and the density ρ on the dynamical behavior. In general, the gel regions I and I_b persist down to the lowest values of τ, but the process of gel aggregation becomes slower as τ decreases. The active labyrinthine region III is not

modified by changes in τ. We focus on the behavior of the MIPS states in Fig. 6, where we plot heat maps of C_L as a function of ρ versus τ. In the frustrated MIPS region IV, shown in Fig. 6(a) at $J = -2$ and $K = -0.001$, MIPS only occurs for the highest densities and activities, indicating that the frustration interferes with the emergence of the MIPS. For the standard MIPS region II with $J = 0$ and $K = 0$, plotted in Fig. 6(b), MIPS extends down to a minimum density of $\rho = 0.4$ and a minimum run time of $\tau = 5 \times 10^4$, spanning a much larger window of ρ and τ than the frustrated MIPS region IV. MIPS is enhanced for the superlattice MIPS region V in Fig. 6(c), where $J = 1$ and $K = -0.01$. The superlattice ordering illustrated in Fig. 3(g) stabilizes the MIPS clusters and allows them to persist down to lower values of τ. The greatest enhancement of C_L occurs in region V_b, shown in Fig. 6(d) at $J = 2$ and $K = -0.001$. For these parameters, the system is not far from the arrested gel region I_b and the regular MIPS region II. Although the long range crystalline ordering of the superlattice found in the superlattice MIPS region V is absent, there is a longer range correlation of the values of ϕ_i within the clustered areas, as illustrated in Fig. 4(d). Neighboring disks have different phases ϕ_i, but next-neighbor disks at a distance $r_{ij} = 4R_d$ have matching values of ϕ_i and tend to stabilize the cluster. This allows the disks in the gas phase to adhere more readily to the surface of the largest cluster since it is not necessary for them to attach at the precise location that would be required if long range ordering were present. As a result, the window of large C_L is maximized for the frustrated cluster fluid region V_b.

IV. DISCUSSION AND SUMMARY

Our active matter swarmalator model demonstrates that ordinary MIPS can be considered as a special case of a larger class of possible active phase separating behaviors. The internal phase degree of freedom of each disk couples to the swarmalator rules and produces additional repulsive and attractive interactions between disks that can compete with or facilitate MIPS formation.
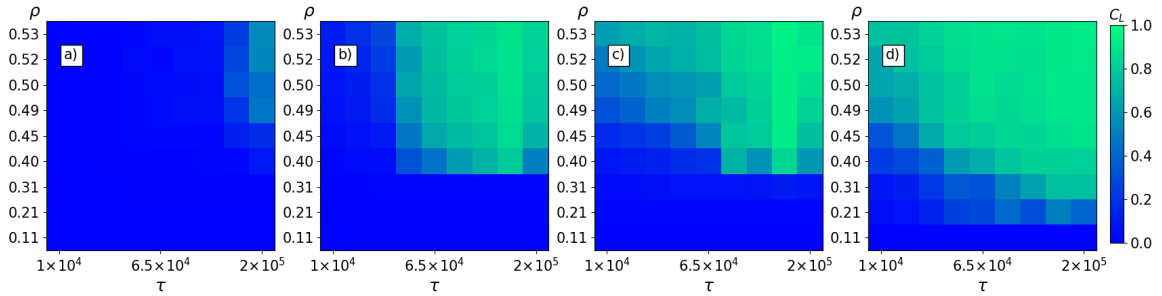
FIG. 6. Behavior of the different MIPS and cluster regimes illustrated with heat maps of the fraction C_L of disks in the largest cluster plotted as a function of disk density ρ versus run time τ. (a) The frustrated MIPS region IV at $J = -2$ and $K = -0.001$. (b) The regular MIPS region II at $J = 0$ and $K = 0$. (c) The superlattice MIPS region V at $J = 1$ and $K = -0.01$. (d) The frustrated cluster fluid region V_b at $J = 2$ and $K = -0.001$.

The swarmalator model generates a wide variety of active phases, including an aggregating gel where activity speeds up aggregation, a phase arrested active gel, regular MIPS, frustrated MIPS with stripe phase ordering, a superlattice phase ordered MIPS, and several correlated active fluids with local phase ordering. Future investigations could address whether there are additional dynamics within the phase-ordered solids, such as periodic oscillations or propagating phase waves. Additional dynamic behaviors could arise if a periodic external driving force were coupled to the internal phase of the disks. Previously considered modifications to generic swarmalator models, such as temperature [50, 51] or chirality [52], could also be introduced to the active disk system. In addition, instead of a continuously variable internal phase, the internal phase could be limited to discrete values in order to draw parallels with Ising or other spin systems. Our results are relevant to active colloidal systems with competing interactions, biological systems with particle-specific interactions, and robotic swarms. This work provides a model for interactions between frustrated systems and the MIPS state, and shows that in some cases, the frustration works against formation of MIPS, but under other conditions, the frustration can instead enhance MIPS.

ACKNOWLEDGMENTS

[1] M. C. Marchetti, J. F. Joanny, S. Ramaswamy, T. B. Liverpool, J. Prost, M. Rao, and R. A. Simha, Hydrodynamics of soft active matter, Rev. Mod. Phys. **85**, 1143 (2013).

[2] C. Bechinger, R. Di Leonardo, H. Löwen, C. Reichhardt, G. Volpe, and G. Volpe, Active particles in complex and crowded environments, Rev. Mod. Phys. **88**, 045006 (2016).

[3] G. Gompper, R. G. Winkler, T. Speck, A. Solon, C. Nardini, F. Peruani, H. Löwen, R. Golestanian, U. Benjamin Kaupp, L. Alvarez, T. Kiørboe, E. Lauga, W. C. K. Poon, A. DeSimone, S. Muiños-Landin, A. Fischer, N. A. Söker, F. Cichos, R. Kapral, P. Gaspard, M. Ripoll, F. Sagues, A. Doostmohammadi, Y. M. Yeomans, I. S. Aranson, C. Bechinger, H. Stark, C. K. Hemelrijk, F. J. Nedelec, T. Sarkar, T. Aryaksama, M. Lacroix, G. Duclos, V. Yashunsky, P. Silberzan, M. Arroyo, and S. Kale, The 2020 motile active matter roadmap, J. Phys.: Condens. Matter **32**, 193001 (2020).

[4] E. Lauga and T. R. Powers, The hydrodynamics of swimming microorganisms, Rep. Prog. Phys. **72**, 096601 (2009).

[5] R. Di Leonardo, L. Angelani, D. Dell'Arciprete, G. Ruocco, V. Iebba, S. Schippa, M. P. Conte, F. Mecarini, F. De Angelis, and E. Di Fabrizio, Bacterial ratchet motors, Proc. Natl. Acad. Sci. (USA) **107**, 9541 (2010).

[6] T. Bhattacharjee and S. S. Datta, Confinement and activity regulate bacterial motion in porous media, Soft Matter **15**, 9920 (2019).

[7] G. Wang, T. V. Phan, S. Li, M. Wombacher, J. Qu, Y. Peng, G. Chen, D. I. Goldman, S. A. Levin, R. H. Austin, and L. Liu, Odd dynamics of living chiral crystals, Nature **607**, 287 (2022).

[8] O. Hallatschek, S. S. Datta, K. Drescher, J. Dunkel, J. Elgeti, B. Waclaw, and N. S. Wingreen, Proliferating active

matter, Nat. Rev. Phys. **5**, 407 (2023).

[9] D. Helbing, Traffic and related self-driven many-particle systems, Rev. Mod. Phys. **73**, 1067 (2001).

[10] C. Castellano, S. Fortunato, and V. Loreto, Statistical physics of social dynamics, Rev. Mod. Phys. **81**, 591 (2009).

[11] M. J. Bowick, N. Fakhri, M. C. Marchetti, and S. Ramaswamy, Symmetry, thermodynamics, and topology in active matter, Phys. Rev. X **12**, 010501 (2022).

[12] S. Shankar, A. Souslov, M. J. Bowick, M. C. Marchetti, and V. Vitelli, Topological active matter, Nat. Rev. Phys. **4**, 380 (2022).

[13] M. Rubenstein, A. Cornejo, and R. Nagpal, Programmable self-assembly in a thousand-robot swarm, Science **345**, 795 (2014).

[14] G. Wang, T. V. Phan, S. Li, M. Wombacher, J. Qu, Y. Peng, G. Chen, D. I. Goldman, S. A. Levin, R. H. Austin, and L. Liu, Emergent field-driven robot swarm states, Phys. Rev. Lett. **126**, 108002 (2021).

[15] M. Y. Ben Zion, J. Fersula, N. Bredeche, and O. Dauchot, Morphological computation and decentralized learning in a swarm of sterically interacting robots, Sci. Robotics **8**, eabo6140 (2023).

[16] Y. Fily and M. C. Marchetti, Athermal phase separation of self-propelled particles with no alignment, Phys. Rev. Lett. **108**, 235702 (2012).

[17] G. S. Redner, M. F. Hagan, and A. Baskaran, Structure and dynamics of a phase-separating active colloidal fluid, Phys. Rev. Lett. **110**, 055701 (2013).

[18] J. Palacci, S. Sacanna, A. P. Steinberg, D. J. Pine, and P. M. Chaikin, Living crystals of light-activated colloidal surfers, Science **339**, 936 (2013).

[19] I. Buttinoni, J. Bialké, F. Kümmel, H. Löwen, C. Bechinger, and T. Speck, Dynamical clustering and phase separation in suspensions of self-propelled colloidal particles, Phys. Rev. Lett. **110**, 238301 (2013).

[20] J. Bialké, J. T. Siebert, H. Löwen, and T. Speck, Negative interfacial tension in phase-separated active Brownian particles, Phys. Rev. Lett. **115**, 098301 (2015).

[21] M. E. Cates and J. Tailleur, Motility-induced phase separation, Ann. Rev Condens. Matter Phys. **6**, 219 (2015).

[22] F. Ginot, I. Theurkauff, F. Detcheverry, C. Ybert, and C. Cottin-Bizonne, Aggregation-fragmentation and individual dynamics of active clusters, Nature Commun. **9**, 696 (2018).

[23] M. Paoluzzi, D. Levis, and I. Pagonabarraga, From motility-induced phase-separation to glassiness in dense active matter, Commun. Phys. **5**, 111 (2022).

[24] A. K. Omar, H. Row, S. A. Mallory, and J. F. Brady, Mechanical theory of nonequilibrium coexistence and motility-induced phase separation, Proc. Natl. Acad. Sci. (USA) **120**, e2219900120 (2023).

[25] M. Seul and D. Andelman, Domain shapes and patterns - the phenomenology of modulated phases, Science **267**, 476 (1995).

[26] G. Malescio and G. Pellicane, Stripe phases from isotropic repulsive interactions, Nature Mater. **2**, 97 (2003).

[27] M. A. Glaser, G. M. Grason, R. D. Kamien, A. Kosmrlj, C. D. Santangelo, and P. Ziherl, Soft spheres make more mesophases, EPL **78**, 46004 (2007).

[28] Q. Chen, S. C. Bae, and S. Granick, Directed self-assembly of a colloidal kagome lattice, Nature (London) **469**, 381 (2011).

[29] K. S. Khalil, A. Sagastegui, Y. Li, M. A. Tahir, J. E. Socolar, B. J. Wiley, and B. B. Yellen, Binary colloidal structures assembled through Ising interactions, Nature Commun. **3**, 794 (2012).

[30] Y. Wang, Y. Wang, D. R. Breed, V. N. Manoharan, L. Feng, A. D. Hollingsworth, M. Weck, and D. J. Pine, Colloids with valence and specific directional bonding, Nature **491**, 51 (2012).

[31] L. Pauling, The structure and entropy of ice and of other crystals with some randomness of atomic arrangement, J. Am. Chem. Soc. **57**, 2680 (1935).

[32] Y. Han, Y. Shokef, A. M. Alsayed, P. Yunker, T. C. Lubensky, and A. G. Yodh, Geometric frustration in buckled colloidal monolayers, Nature (London) **456**, 898 (2008).

[33] A. Ortiz-Ambriz and P. Tierno, Engineering of frustration in colloidal artificial ices realized on microfeatured grooved lattices, Nature Commun. **7**, 10575 (2016).

[34] A. P. Ramirez, Geometric frustration: Magic moments, Nature **421**, 483 (2003).

[35] C. Nisoli, R. Moessner, and P. Schiffer, Colloquium: Artificial spin ice: Designing and imaging magnetic frustration, Rev. Mod. Phys. **85**, 1473 (2013).

[36] S. H. Skjærvø, C. H. Marrows, R. L. Stamps, and L. J. Heyderman, Advances in artificial spin ice, Nat. Rev. Phys. **2**, 13 (2020).

[37] X. Guo, M. Guzmán, D. Carpentier, D. Bartolo, and C. Coulais, Non-orientable order and non-commutative response in frustrated metamaterials, Nature **618**, 506 (2023).

[38] K. P. O'Keeffe, H. Hong, and S. H. Strogatz, Oscillators that sync and swarm, Nature Commun. **8**, 1504 (2017).

[39] A. Barciś, M. Barciś, and C. Bettstetter, Robots that sync and swarm: A proof of concept in ROS 2, in *2019 International Symposium on Multi-Robot and Multi-Agent Systems (MRS)* (2019) pp. 98–104.

[40] S. Ceron, G. Gardi, K. Petersen, and M. Sitti, Programmable self-organization of heterogeneous microrobot collectives, Proc. Natl. Acad. Sci. (USA) **120**, e2221913120 (2023).

[41] Y. Jiao, T. Lau, H. Hatzikirou, M. Meyer-Hermann, J. C. Corbo, and S. Torquato, Avian photoreceptor patterns represent a disordered hyperuniform solution to a multiscale packing problem, Phys. Rev. E **89**, 022721 (2014).

[42] E. A. Jagla, Phase behavior of a system of particles with core collapse, Phys. Rev. E **58**, 1478 (1998).

[43] C. J. Olson Reichhardt, C. Reichhardt, and A. R. Bishop, Structural transitions, melting, and intermediate phases for stripe- and clump-forming systems, Phys. Rev. E **82**, 041502 (2010).

[44] E. Pince, S. K. P. Velu, A. Callegari, P. Elahi, S. Gigan, G. Volpe, and G. Volpe, Disorder-mediated crowd control in an active matter system, Nature Commun. **7**, 10907 (2016).

[45] F. A. Lavergne, H. Wendehenne, T. Baeuerle, and C. Bechinger, Group formation and cohesion of active particles with visual perception-dependent motility, Science **364**, 70 (2019).

[46] T. Bäuerle, R. C. Löffler, and C. Bechinger, Formation of stable and responsive collective states in suspensions of active colloids, Nature Commun. **11**, 2547 (2020).

[47] Y. Shokef and T. C. Lubensky, Stripes, zigzags, and slow dynamics in buckled hard spheres, Phys. Rev. Lett. **102**, 048303 (2009).

[48] A. Hill, M. Tanaka, K. B. Aptowicz, C. K. Mishra, A. G. Yodh, and X. Ma, Depletion-driven antiferromagnetic, paramagnetic, and ferromagnetic behavior in quasi-two-dimensional buckled colloidal solids, J. Chem. Phys. **158**, 194903 (2023).

[49] S. Luding and H. J. Herrmann, Cluster-growth in freely cooling granular media, Chaos **9**, 673 (1999).

[50] G. K. Sar and D. Gosh, Dynamics of swarmalators: A pedagogical review, EPL **139**, 53001 (2022).

[51] H. Hong, K. P. O'Keeffe, J. S. Lee, and H. Park, Swarmalators with thermal noise, Phys. Rev. Res. **5**, 023105 (2023).

[52] S. Ceron, K. O'Keeffe, and K. Petersen, Diverse behaviors in non-uniform chiral and non-chiral swarmalators, Nature Commun. **14**, 940 (2023).